Effect of lateral outflow on three-dimensional flow structure in a river delta

M. Kifayath Chowdhury [1,4], Kory M Konsoer [2,3], Matthew Hiatt[1,3]

[1]Department of Oceanography and Coastal Sciences, College of the Coast and Environment, Louisiana State University, Baton Rouge, LA, USA
[2]Department of Geography, Louisiana State University, Baton Rouge, LA, USA
[3]Coastal Studies Institute, Louisiana State University, Baton Rouge, LA, USA
[4]Now at Faculty of Civil Engineering and Geosciences, Delft University of Technology, Delft, Netherlands

Key Points:

- Channelized outflow was observed to induce coherent secondary circulations while unchannelized lateral outflow did not.
- Formation of the coherent secondary circulations may depend upon available lateral momentum flux and length scale of outflow in the channel.
- Suspended sediment transport to wetlands may depend on strength of secondary circulation cells.

Corresponding author: Matthew Hiatt, mhiatt1@lsu.edu

Abstract

Spatial and temporal patterns in three-dimensional flow structure are linked to channel processes and morphology in many environments. However, there is not yet an understanding of how the flow structure is influenced by channelized and gradually distributed lateral outflows that are often prevalent in river deltas. This study presents an analysis of three-dimensional flow structure data collected from Wax Lake Delta, a naturally developing river-dominated delta in the northern Gulf of Mexico. Three hydrographic surveys were conducted using a boat-mounted acoustic Doppler current profiler at two sites: a channelized outflow zone and a distributary channel experiencing unchannelized lateral outflow. The flow structure was analyzed to identify secondary circulation cells induced by both types of lateral outflow. For channelized outflow, coherent cells were observed. However, minimal presence of coherent structures was observed for unchannelized lateral outflow. The results suggest that the formation of detectable secondary circulation cells may depend upon a threshold value of the ratio of the lateral momentum flux along the length of the outflow zone and primary flow momentum flux. The threshold lies in between 0.211 km^{-1} and 0.375 km^{-1} for the conditions tested. This research contributes novel field measurements of flow structure in an actively prograding river delta and offers important implications for coastal restoration by linking three-dimensional flow structure to lateral outflow.

Plain Language Summary

A developing river delta consists of channels that distribute water and sediment and islands that are in the process of formation and remain partially flooded. Water moves from distributary channels onto these islands laterally through smaller channels or over the channel bank. Sediment and nutrients also get carried from the channels onto the delta islands, which is important for the health and growth of the delta. Understanding the physics of the water movement helps scientists understand how deltas build land and allows for improved or more robust restoration projects. Here we use an acoustic instrument called an acoustic Doppler current profiler to measure the complex patterns of water velocity created by the water flow through small channels and over banks in a river delta. We observe strong rotating flow in the channels when the water outflows through a side channel. However, weak rotating flow was observed when the water gets distributed over a large area through flow over the bank. The results suggest the strength and type of lateral outflow (either through a channel or over the bank) control whether or not rotating flows can form. The results of this study have implications for better understanding water movement and the evolution of river deltas.

1 Introduction

Deltaic environments are known to exhibit hydraulic connectivity between distributary channels and interdistributary islands through lateral outflow (Hiatt & Passalacqua, 2015). Velocity and sediment transport in these lowermost reaches of rivers are significantly modulated by the discharge lost through lateral outflow (Esposito et al., 2020; Hiatt & Passalacqua, 2017), indicating that lateral hydraulic connectivity exerts a considerable influence on the morphodynamic evolution of river deltas (Coffey & Shaw, 2017; Shaw et al., 2016). Though it is understood that internal conditions (topobathymtery and vegetation) and external forces (riverine discharge, tides, winds, and storm events) determine the magnitude and direction of hydraulic connectivity in deltas (Hiatt & Passalacqua, 2015; Hiatt et al., 2018; Passalacqua, 2017; Olliver et al., 2020; Wright et al., 2018), less is known about the flow structure, or three-dimensional hydrodynamic patterns, resulting from lateral outflow.

Lateral outflow between the interdistributary channels and islands of a river delta takes on one of two forms: 1) channelized lateral outflow (CO) through a secondary channel or crevasse, and 2) unchannelized lateral outflow (UO) via overbank flow onto the interdistributary island bay or floodplain (Hiatt & Passalacqua, 2015; Shaw et al., 2013). It has been shown that the distributary channel system of Wax Lake delta (Louisiana, USA) loses approximately 24-50% of discharge through lateral outflow to the islands (Hiatt & Passalacqua, 2015, 2017; Hiatt et al., 2018; Shaw et al., 2016) and the mechanism may also influence the transport of suspended sediments to the islands (Bevington & Twilley, 2018; Olliver et al., 2020; Shaw et al., 2016). Such exchange between channels and deltaic floodplains is known to be modulated by geometry, river discharge, tides, wind, storms, and the presence of vegetation, among others (Hiatt & Passalacqua, 2015, 2017; Passalacqua, 2017; O'Connor & Moffett, 2015; Olliver et al., 2020) and it is likely that the resulting three-dimensional flow structure will be influenced by similar factors.

Flow structure provides information regarding the interaction of primary and secondary components of velocity. These secondary components of three-dimensional flow can represent the existence of secondary currents. One of the two types of secondary currents generally observed is generated due to flow curvature through the imbalance between the centrifugal force and the transverse pressure gradient, also known as Prandtl's first kind. The center region cell observed in curved channels with longitudinal axis along the main flow direction (Blanckaert & Vriend, 2004) is an example of this type. The secondary current of first kind plays a significant role in distribution of streamwise momentum when the radius of curvature is small (Uijttewaal, 2014). The other type, commonly known as secondary circulations of Prandtl's second kind, is steered by the anisotropy of turbulence with axes of rotation parallel to the mean flow. An example is the secondary outer bank cell generally observed in the outer bank of a curved channel driven by both turbulence and centrifugal force (Blanckaert & Vriend, 2004). Secondary currents can be either coherent or incoherent.

Laboratory experiments and numerical modeling have demonstrated that different secondary circulations develop in channel systems where lateral outflow takes place, for instance, in diversions (Bulle, 1926; Herrero et al., 2015; Neary & Odgaard, 1993; Neary et al., 1999), bifurcations (Hardy et al., 2011; Marra et al., 2014; Miori et al., 2012; Thomas et al., 2011), side weirs (Michelazzo et al., 2015), and compound channels with floodplain (Proust & Nikora, 2019; Tominaga & Nezu, 1991). However, field measurements of three-dimensional flow structure are typically limited to fluvial systems like meander bends (Engel & Rhoads, 2017; Frothingham & Rhoads, 2003; Konsoer et al., 2016; Sukhodolov, 2012; Zinger et al., 2013; Finotello et al., 2020), confluences (Serres et al., 1999; Szupiany et al., 2009), and bedrock canyons (Venditti et al., 2014). Observations at tidally-influenced deltaic bifurcations (Buschman et al., 2013; Sassi et al., 2013; Kästner & Hoitink, 2019) have identified key controls on three-dimensional flow structure in channelized outflows, but observations of the impact of outflow type (CO versus UO) remain elusive, despite the importance of the channelized-unchannelized flow transition in river deltas (Hiatt & Passalacqua, 2017; Coffey & Shaw, 2017) and advancements in characterizing two-dimensional transport processes in prograding deltas like Wax Lake delta (WLD) (Shaw et al., 2018; Olliver et al., 2020; Christensen et al., 2020).

In river deltas, channelized lateral outflow usually takes the form of high-angle secondary channels connecting main distributary channels to inundated interdistributary interiors (Shaw et al., 2013). Open channel diversions are analogous to such channelized lateral outflow. At 90° lateral diversions, secondary circulations have been observed in the main and lateral channel (Dutta et al., 2017; Herrero et al., 2015; Neary & Odgaard, 1993; Neary et al., 1999; Ramamurthy et al., 2007). For a diversion on the left bank (looking downstream), two counter rotating cells were observed, one rotating clockwise inside the lateral channel and another rotating counterclockwise located downstream of the diversion in the main channel (Neary et al., 1999). An imbalance between the transverse pressure gradient, shear, and centrifugal forces along the vertical is the primary reason behind the cells at a diversion (Neary et al., 1999). However, Miori et al. (2012) demonstrated that for bifurcations, these counter-rotating cells form upstream of the bifurcation apex and later extend into the downstream branches. Recently, Herrero et al. (2015) proposed that the strength of secondary circulation downstream of the diversion depends on the momentum flux associated with lateral outflow. However, this proposal is specific for only one observed cell and considers neither the geometry of the outflow section nor other circulations that exist simultaneously in the system.

Nearly all of the 90° diversion studies focus on non-discordant systems where the main and lateral channels have the same bed elevation. However, bifurcations in nature often show discordance (Zolezzi et al., 2006), and flow structures are somewhat affected by them (Miori et al., 2012). Side weirs generally resemble the flow in such discordant environment. Main channel bedform morphology has been observed to be influenced by the lateral outflow through side weirs (Michelazzo et al., 2016; Paris et al., 2012; Rosier et al., 2011). According to Michelazzo et al. (2016), 3-D eddies form at the mouth of side weirs and act to divert sediment into the weirs. Despite these efforts in open channel hydraulics, there remains a gap between the understanding of flow and transport mechanism from the hydrodynamic models (Dutta et al., 2017) and the more morphology focused studies (Szewczyk et al., 2020) for channelized systems. Moreover, there remains a lack of understanding of how flow structure in discordant systems is modulated by environmental variables such as tides and discharge.

Unchannelized outflow (UO) occurs when water flows laterally over subaqueous channel levees into the floodplain or interdistributary bay of a river delta. UO is analogous to compound channel flow studied in fluvial settings. The characteristics of compound channel flow structure are recognized by the flow specifically in the junction between main channel and floodplain (Tominaga & Nezu, 1991). Shear induced horizontal eddy structures like the Kelvin-Helmholtz instability and turbulence-induced secondary circulations (Prandtl's second kind) were observed at such junctions (Tominaga & Nezu, 1991). Secondary current intensity and vortex size depend on the Froude number, roughness (Nezu & Onitsuka, 2001), and the depth ratio between the floodplain and main channel (Proust & Nikora, 2019; Tominaga & Nezu, 1991). Additionally, the direction of transverse currents was found to be a crucial control over the orientation of turbulence induced secondary currents in compound channels (Proust & Nikora, 2019). Deltaic systems generally have tidal influence to varying extents, and hydraulic connectivity between channels and floodplains in WLD has been shown to depend on tides (Christensen et al., 2020), lending credence to the hypothesis that tides will impact transverse currents and secondary flow structure. However, field data addressing this remains lacking.

The current study analyzes 3-D flow structure induced by lateral outflow from delta distributary channels and establishes a conceptual representation of flow structure due to lateral outflow. The research aims to: 1) characterize the three-dimensional flow structures that appear in channelized and unchannelized lateral outflow within delta distributary channels; and 2) develop a quantitative measure to predict the presence of coherent circulation cells induced by CO and UO. We conduct this work in the well-studied WLD, which is often viewed as a prototype for land-building efforts through sediment diversions, which are currently proposed as the primary land-building mechanism in the Lower Mississippi River Delta (CPRA, 2017). The results from this study have implications for understanding and evaluating the hydrodynamics and sediment transport processes in deltaic systems and also for bifurcations in a suspended load dominated environment. This may be used to evaluate the efficacy of sediment diversions at reproducing the processes of land-building deltas in addition to aiding in design and operation strategies.

2 Methods

2.1 Site description

WLD is a river dominated delta located in coastal Louisiana at the mouth of the 25 km long Wax Lake Outlet (WLO) (Fig. 1a). WLD debouches into the Atchafalaya Bay about 140 km West-Southwest of New Orleans (Fig. 1b). The outlet was dredged by US Army Corps of Engineers in 1942 with a design capacity to carry 30% of the discharge from the Atchafalaya River to reduce flooding in Morgan City, LA (Roberts et al., 2003). Sediment began to deposit at the mouth of WLO immediately after construction and WLD has been steadily prograding since its first subaerial emergence in 1973 (Roberts et al., 1997). Sediment input to WLD is estimated to be 38.4 Mt/year, 18% of which is sand (Kim et al., 2009). Estimates of the delta land growth rate and the total area of land built provided by the literature are variable but it is estimated that approximately over 100 km^2 new deltaic surface has been developed at WLD since its subaerial emergence in 1973 (Roberts, 1998; Wellner et al., 2005). Water levels are modulated by mixed semidiurnal microtides (mean range of 0.35 m) and the average flow in WLO is 3078 m^3/s while the annual flood tends to peak above 5000 m^3/s (Hiatt & Passalacqua, 2015).

WLD hosts a branching distributary network with seven major channels and partially-inundated interdistributary islands. The channel network of WLD consists of primary (>100 m width) and lateral secondary channels. Primary channels distribute the water and sediment throughout the system and secondary channels connect the primary channels to the island interiors. The delta islands are typically shaped like an arrowhead and are surrounded by narrow levees with higher elevation. The distributary channels are lined with these levees which can be subaerial or subaqueous based on the water level. Flow over the levees resulting in flow exchange between the channels and islands is a persistent feature of the system. The sedimentary framework of WLD is 50-70% medium sand (Roberts et al., 1997). The D_{50} and D_{90} (50th and 90th percentiles of grain size) range of suspended sand at WLD apex are respectively 98-106 μm and 138-175 μm (Shaw et al., 2013). The Froude number of flow entering the delta is $\sim$ 0.25 during bankfull flow (Edmonds et al., 2011).

In this study, the flow structure was measured at a site experiencing CO and along a distibrutary channel subject to UO (Fig. 1c-d). The CO study site was located at Mallard Pass, a distributary channel in the western part of WLD, 2.3 km downstream of the channel entrance (Fig. 1c). The secondary channel is located at the outer bank of a mild curvature and flows laterally into an interdistributary island and has been relatively stable since 2000. Overall seaward migration of the channel was approximately 30-50 m and lateral migration was approximately 120 m between 2000-2020. At WLD, UO has been primarily observed along distributary channels near the delta front and generally takes the form of lateral overbank flow (Hiatt & Passalacqua, 2015; Shaw et al., 2016). To capture this phenomenon, a 3.7 km long section of Gadwall Pass was surveyed in this study (Fig. 1d).

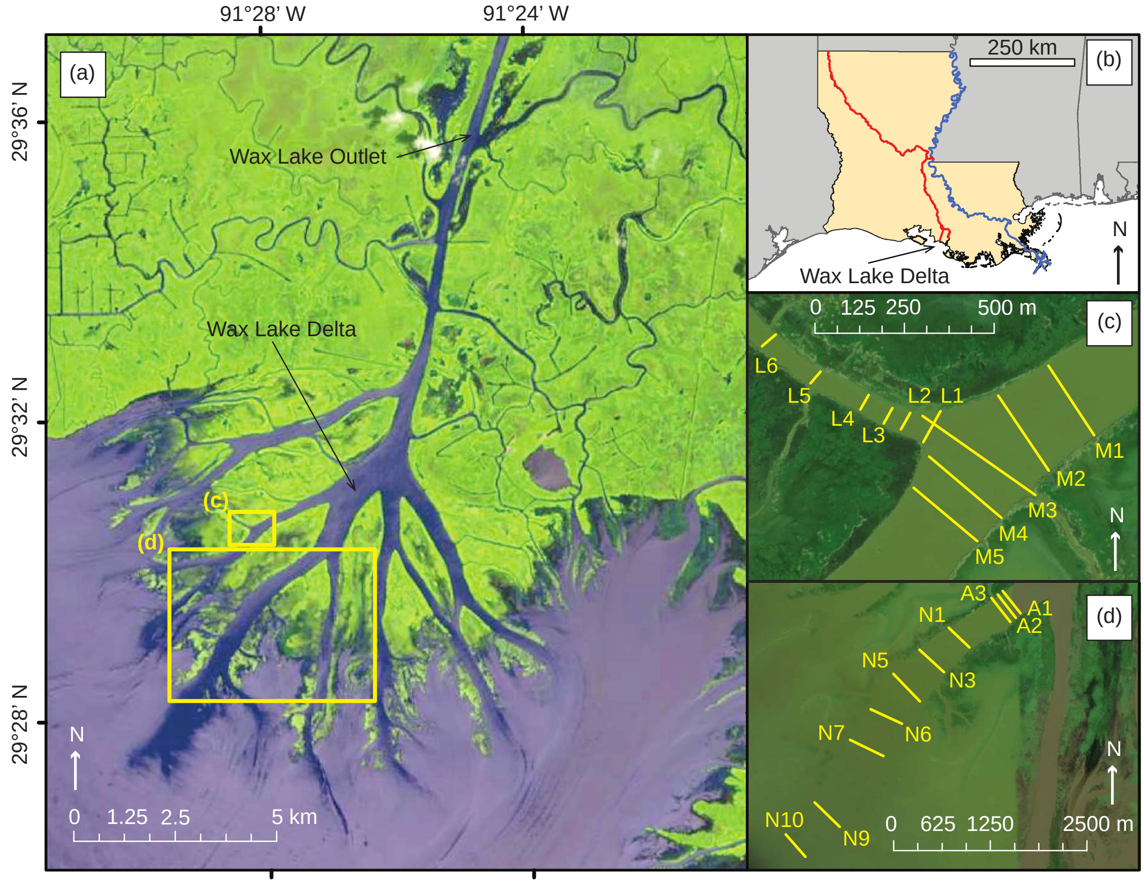

Figure 1. (a) Map of the study region depicting Wax Lake Delta (WLD) and Wax Lake Outlet (WLO). Locations of ADCP transects traversed in Mallard Pass (15 April and 10 June 2019) and in Gadwall Pass (9 June and 13-14 September 2019) are marked by yellow rectangles. (b) Map of the study site within Louisiana (USA). WLD receives flow through the WLO, a dredged flood control outlet of the Atchafalaya River (delineated in red along with the Red River). The Mississippi River is delineated in blue. (c) ADCP transect locations of the channelized outflow (CO) system in Mallard Pass. (d) ADCP transect locations of Gadwall pass where unchannelized outflow (UO) was observed. Image specification for (a): Landsat 8 30m resolution satellite image from June 2019 (available online at https://earthexplorer.usgs.gov/). Image specifications for (c) and (d): Maxar Vivid image from March 8, 2021 at 0.5 m resolution accessed through ArcGIS Online.

2.2 Data collection

The field measurements at WLD comprised three trips from April 2019 to September 2019. Time series plots of discharge at WLO (USGS Gauge # 07381590 in Calumet) and water-level (NOAA Lawma-Amerada Pass station # 8764227) in the water year 2019 are provided in Fig. 2, which indicates the conditions during each set of measurements.

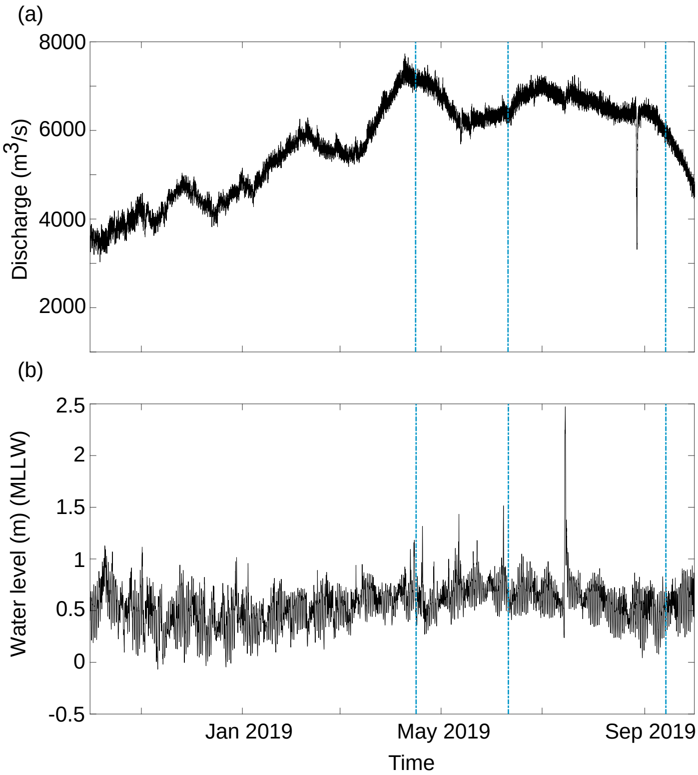

Figure 2. (a) Discharge in the Wax Lake Outlet at the USGS Gauge # 07381590 in Calumet, LA. (b) Measured water-level at the NOAA Lawma-Amerada Pass station (NOAA # 8764227) during water year 2019, blue verticals indicate survey periods.

A 1200 kHz Teledyne RDI RiverPro acoustic Doppler current profiler (ADCP) was used for the hydrographic surveys. The RiverPro is a 5 beam system with one vertical beam and four beams at 20 degrees. All measurements were georeferenced using an external Hemisphere A101 differential Global Positioning System (dGPS) mounted over the ADCP. The ADCP transducer depth was kept at 0.3 m with a blanking distance of 0.25 m from the sensor head. Data from the measurement bins close to the bottom were ignored automatically by the ADCP's auto-adaptive system to avoid sidelobe interference. Bin size for each ensemble is optimized by an auto-adaptive system of the ADCP that yielded cell size ranging from $2-24$ cm depending on the depth of that ensemble. The water mode was selected automatically based on the flow condition. The velocity resolution of the ADCP is 1 mm/s with an accuracy within $\pm$ 0.25% of water velocity relative to the ADCP. At least four repeat transects were performed to collect multiple velocity measurements along the georeferenced cross-sections (Fig. 1) based on community recommendations (Szupiany et al., 2007) and USGS standards for hydrographic surveys (Mueller et al., 2013). When possible, the same georeferenced cross-sections were surveyed during each measurement campaign, but due to the evolving channel planform and navigability, slight reorientation of some transects was necessary.

Velocity and discharge data from the CO zone were collected during falling tide on 15 April 2019 and during rising tide on 10 June 2019. On 15 April (campaign 1), hydrographic measurements were performed at five transects spaced approximately 100 m apart in the main channel (M1-M5) and at four transects inside the secondary channel separated by approximately 50 m (L1-L4) (Fig. 1b). The same cross-sections were traversed during the 10 June survey (campaign 2) with two additional transects located further inside the lateral channel (L5 and L6 in Fig. 1b). Because of the historic flooding in the lower Mississippi River in 2019 (Pal et al., 2020), the discharge entering WLD during both the surveys was higher (5584 m^3/s on 15 April and 5944 m^3/s on 10 June) than the average in WLO. A discharge summary from the surveys is provided in the supporting information (Table S1).

For the UO site (Fig. 1c), an initial survey of Gadwall Pass was performed on 9 June 2019 during falling tide to identify the location where lateral outflow begins. Lateral outflow was observed at transect N5 (discharge 1433 m^3/s), and it was found to have $\sim 5\%$ discharge loss relative to the transect 400 m upstream (transect N3, discharge 1510 m^3/s)(Table S1). Thus, N5 represented a reasonable location for the upstream boundary of the lateral outflow zone and was selected as the baseline for the velocity and discharge measurement in September. After the long 2019 flood season (Fig. 2a), the discharge at the delta apex dropped significantly to 2210 m^3/s in September (Table S1). The cross-sections were spaced 500 m apart from each other, starting from N5. One initial discharge measurement survey was performed at the beginning of both the 13 and 14 September surveys at the upstream end of Gadwall Pass. During rising tide, 13 September 2019 (campaign 3), 5 of the selected cross-sections (N5-N7, N9-N10) were traversed. On 14 September 2019 (campaign 4), the cross-sections- N5, N9, and N10, were surveyed during falling tide. Transect N7 was removed from campaign 4 as the discharge variation from each pass of this transect exceeded acceptable error limit (individual discharge measurements were not within 5% of the mean measured discharge (Mueller et al., 2013)). Winds were mostly consistent during the surveys with peak speeds <5 m/s.

2.3 Post processing

ADCP data were collected, reviewed, and exported as ASCII files using WinRiver II® software. For campaigns 1 and 2, the vertical velocity data from the ADCP was found to be negatively biased because of the tilt sensor not functioning properly. Beam velocities from the ADCP were therefore corrected using an in-house code written in Matlab® (Chowdhury, 2020) to account for the effects of tilt, pitch, and roll. Both four-beam and three-beam solutions were taken during the correction (Teledyne, 2010). For campaign 3 and 4, the correction was done using WinRiver II setup wizard with a coordinate transformation user command (Teledyne, 2017). In addition, an ensemble mean removal detrending for the vertical velocity was performed. A comparison between the detrended and biased vertical velocity data is given in the supporting materials (Fig. S1).

The corrected data were then analyzed using Velocity Mapping Toolbox (VMT), a suite of Matlab® routines (Parsons et al., 2013). VMT averages the repeat transects along a cross-section, calculates primary and secondary velocity vectors in multiple frames of references for the mean transect, and allows plotting three-dimensional velocity information for the mean cross-section. For this study, the secondary velocity vectors in Rozovskii frame of reference (Rozovskii, 1957) and the transverse vectors were used. Secondary vectors in the zero secondary discharge reference frame were ignored as all of the cross-sections traversed in this study had a significant amount of lateral outflow, which violates the assumptions of zero net secondary discharge. In the Rozovskii frame of reference, the secondary vectors are rotated such that for each vertical profile, secondary currents in one direction are equal to those in the opposite direction (Lane et al., 2000). In other words, the primary velocity at each vertical in this reference frame is equivalent to the depth-averaged velocity direction at that vertical. Thus the primary velocity direction varies across a section (Lane et al., 2000; Rhoads & Kenworthy, 1998). The Rozovskii frame of reference is useful for identifying helical motion in strongly converging and diverging flows (Rhoads & Kenworthy, 1998; Rozovskii, 1957).

The bathymetry data were interpolated from the ADCP transects. For higher resolution bathymetry, additional zigzag ADCP surveys were performed. These bathymetry data were exported using VMT in UTM coordinates, and a Kriging interpolation was performed in ArcGIS®. The grid size was 10×10 m for the CO system and 20×20 m for the UO sites. The resulting bathymetry was triangulated for visualization in Tecplot 360 (Fig. 3). This method introduces interpolation errors and temporal variation of bed load increases the uncertainty of the resulting spatial distribution (Rennie & Church, 2010). The interpolated bathymetry (Fig. 3) is used only for qualitative assessment of the morphology and visualization.

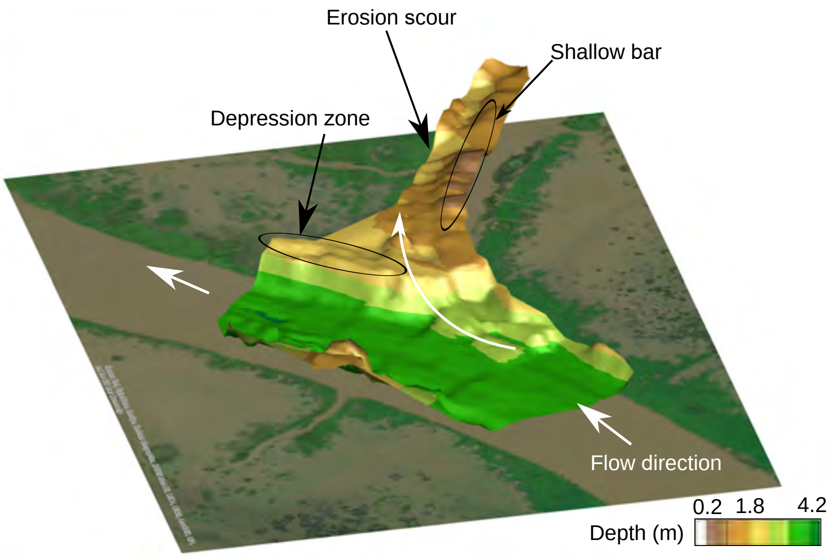

Figure 3. Interpolated bathymetry of the channelized outflow (CO) site produced using ArcGIS® and Tecplot® from the ADCP data collected on June 10, 2019. The grid size used for Kriging in ArcGIS® is 10m.

2.4 Analysis

The momentum flux ratio (M_r) is defined as the ratio of momentum flux (P) between the bifurcating channel and main channel (Herrero et al., 2015). It is calculated as:

$$M_r = \frac{\rho_l Q_l v_l}{\rho_u Q_u v_u} \tag{1}$$

which is the ratio of the product of fluid density (ρ), discharge (Q), and velocity (v) at the mouth of the lateral channel (denoted by subscript l) and at the cross section upstream of lateral channel (denoted by subscript u). M_r has been used as a parameter to characterize bed morphology and flow pattern in confluences (Miyawaki et al., 2010; Rhoads & Sukhodolov, 2001) and 90° diversions (Herrero et al., 2015). Values of M_r were calculated for each of the field surveys both on CO and UO systems (Table 1) with ρ_u

and ρ_l assumed to be equal and Q_u, v_u, Q_l, and v_l extracted from the ADCP data (Table 1). For M_r in the UO case, the following equation is used,

$$M_r = \frac{P_u - P_d}{P_u} \tag{2}$$

where the numerator denotes the momentum flux lost due to lateral outflow to one of the banks for an outflow distance (L). It is calculated by subtracting the momentum flux in the downstream transect (P_d) from the upstream one (P_u).

For the purpose of this study, the momentum flux ratio was divided by the length of the outflow zone along the primary axis of the main channel to yield the momentum flux ratio per unit length of outflow or outflow momentum flux ratio, M_r'. This is done to capture the effects of outflow type (CO or UO) on momentum flux in a single parameter. For CO, the length (L) is the lateral channel width. For UO, the centerline distance between two transects is used for incremental outflow length (L), assuming the outflow occurs only through one channel bank. Eq. 1 thus is modified as,

$$M_r' = \frac{M_r}{L} \tag{3}$$

3 Results

3.1 Channelized lateral outflow

Discharge and flow characteristics

Depth-averaged velocities from the CO surveys identified spatial gradients in velocity throughout the survey site (Fig. 4). The lateral channel captured 6.88% and 5.24% of the discharge in Mallard pass during campaigns 1 and 2, respectively (Table 1).

Primary flow directions for both surveys did not show any significant change with the tide (i.e., no flow reversal occurred). The velocity magnitude into the lateral channel was roughly 50% of that in the primary flow direction in the main channel (Table 1). Separation zones upstream of the lateral channel were observed along both banks (Fig. 4). Moreover, the lateral channel bed was observed to be at a higher elevation than the main channel bed representing a discordant bathymetric feature. No shallow bar was observed in the main channel on the opposite bank of the lateral channel (Fig. 3) likely because of the small discharge ratio with the secondary channel (Neary et al., 1999).

Two zones of flow were observed inside the lateral channel. The flow close to the right bank had a significantly lower velocity than the left bank coinciding with a shallow elongated bar and a cut bank on the left (Fig. 3). The high velocity core in the lateral channel gradually shifted from the left bank to the middle of the channel as the water moved farther inward (Fig. 4). Velocity downstream of the lateral channel farther increased during falling tide and decreased during rising tide (Fig. 4). M_r' varied between 0.375 km^{-1} and 0.492 km^{-1} for the conditions tested (Table 1).

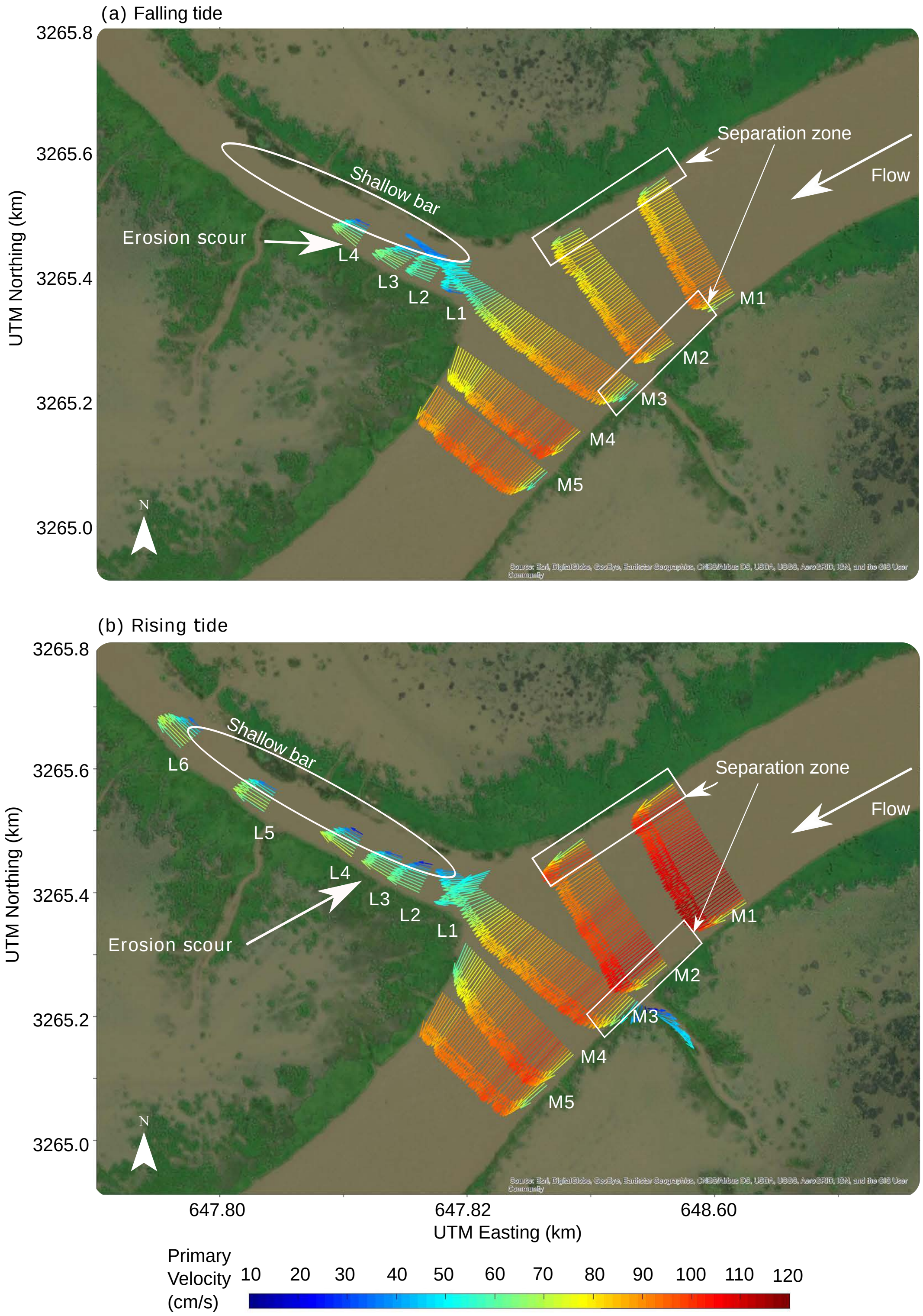

Figure 4. Depth-averaged velocity vectors for channelized outflow during (a) campaign 1, (April 15, 2019), representing the falling tide and (b) campaign 2 (June 10, 2019), representing the rising tide. Field conditions for each set of measurements are contained in Table 1.

Flow structure

The secondary velocity in the Rozovskii reference frame at transect M2 for both rising and falling tide shows a large channel-wide clockwise circulation in the main channel (Fig. 5a). The width of the separation zone at M2 on the right bank was ∼15 m. In the separation zone on the right bank, a coherent counter-clockwise rotating cell was observed both in the falling and rising tide. This coherent cell was observed to exist only in the separation zone upstream and at the mouth of the lateral channel (Fig. 5a and c) and its circulation velocity varied between 2 and 5 cm/s.

The counter-clockwise rotating cell at the discordant bed junction at transect M3 had a maximum helical velocity of 5 cm/s during the falling tide survey (Fig. 5c). The transverse velocity near the lateral channel mouth at M3 during campaigns 1 and 2 were respectively 35% and 30% of mean streamwise velocity.

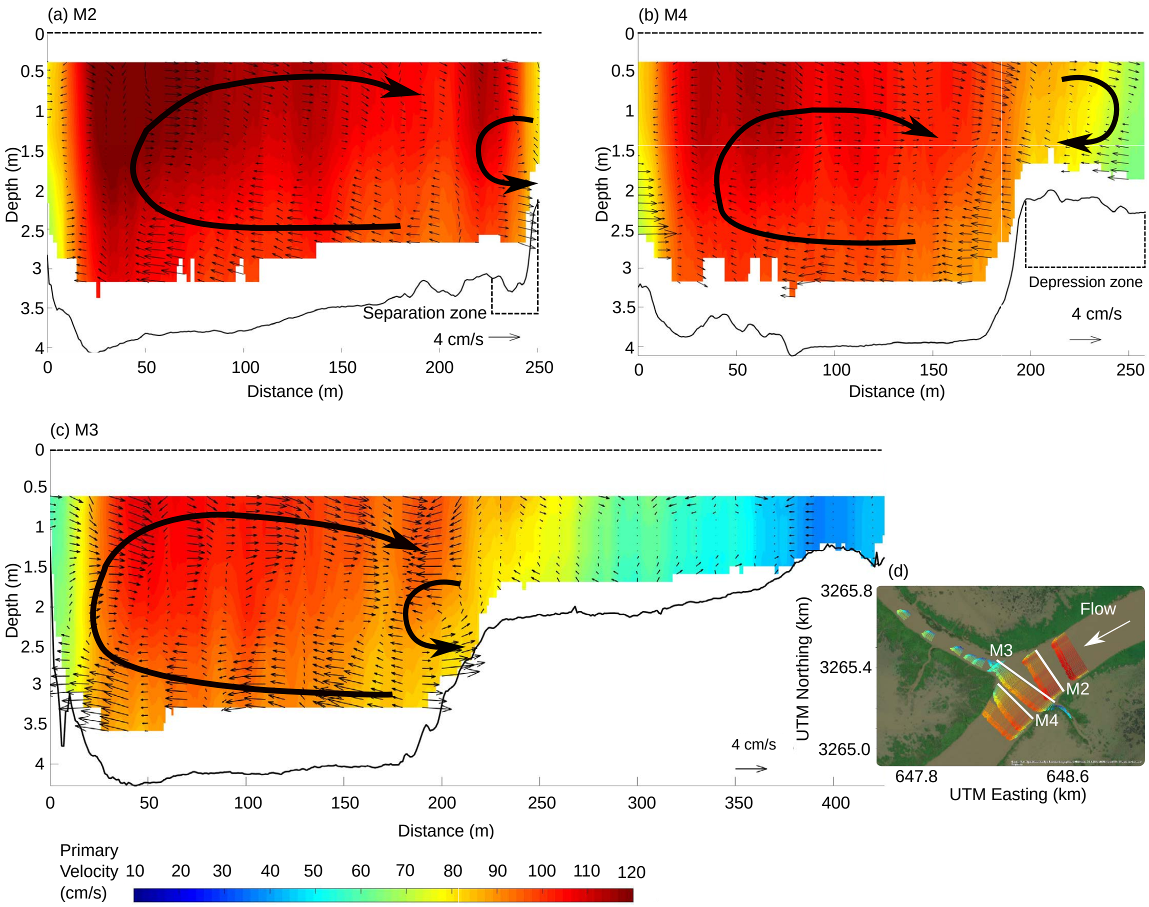

Figure 5. Flow structure at transects (a) M2, (b) M4, and (c) M3 (looking downstream). The contour shows the primary velocity in the downstream direction and secondary velocities in the Rozovskii reference frame are shown by arrows. Transects M2 and M4 are from campaign 2 (rising tide) and transect M3 data is from campaign 1 (falling tide). The inset shows the location of the transects.

The clockwise rotating cell observed at M2 remained the dominant circulation pattern in M3. This dominant channel-wide clockwise secondary circulation also prevailed

Table 1. Channelized Outflow (CO) field results summary

Parameters	**Specification**	Falling tide	Rising tide
Area ratio	L1/M2	0.1283	0.1368
	L1/M4	0.1409	0.1398
Width ratio	L1/M2	0.3290	0.3216
	L1/M4	0.3401	0.3396
Discharge ratio (lateral to upstream)	CO (M2-L1)	0.0688	0.0524
	UO (N5-N9)	0.3	0.3
Width/Depth	L1	50.49	53.25
	M2	66.72	74.30
	M4	69.09	69.65
Mean velocity magnitude (cm/s)	L1	53.30	59.73
	M2	90.70	109.25
	M4	96.64	102.66
	N5	25	21
	N9	23	17
Normalized transect distance with respect to lateral channel width	L1	0.37	0.17
	L2	0.86	1.15
	L3	1.47	1.70
	L4	2.47	2.64
	L5	-	4.47
	L6	-	6.33
Froude Number	L1	0.131	0.151
	M2	0.147	0.185
	M4	0.162	0.173
	N5	0.046	0.038
	N9	0.042	0.031
Momentum flux ratio	CO (M2-L1)	0.04	0.03
	UO (N5-N9)	0.35	0.4
Outflow momentum flux ratio (km^{-1})	CO (M2-L1)	0.492	0.375
	UO (N5-N9)	0.211	0.177

through the transects M4 (Fig. 5b) and M5 (Fig. 6a and 6b) and likely represents the center region cell formed due to the curvature of the main channel.

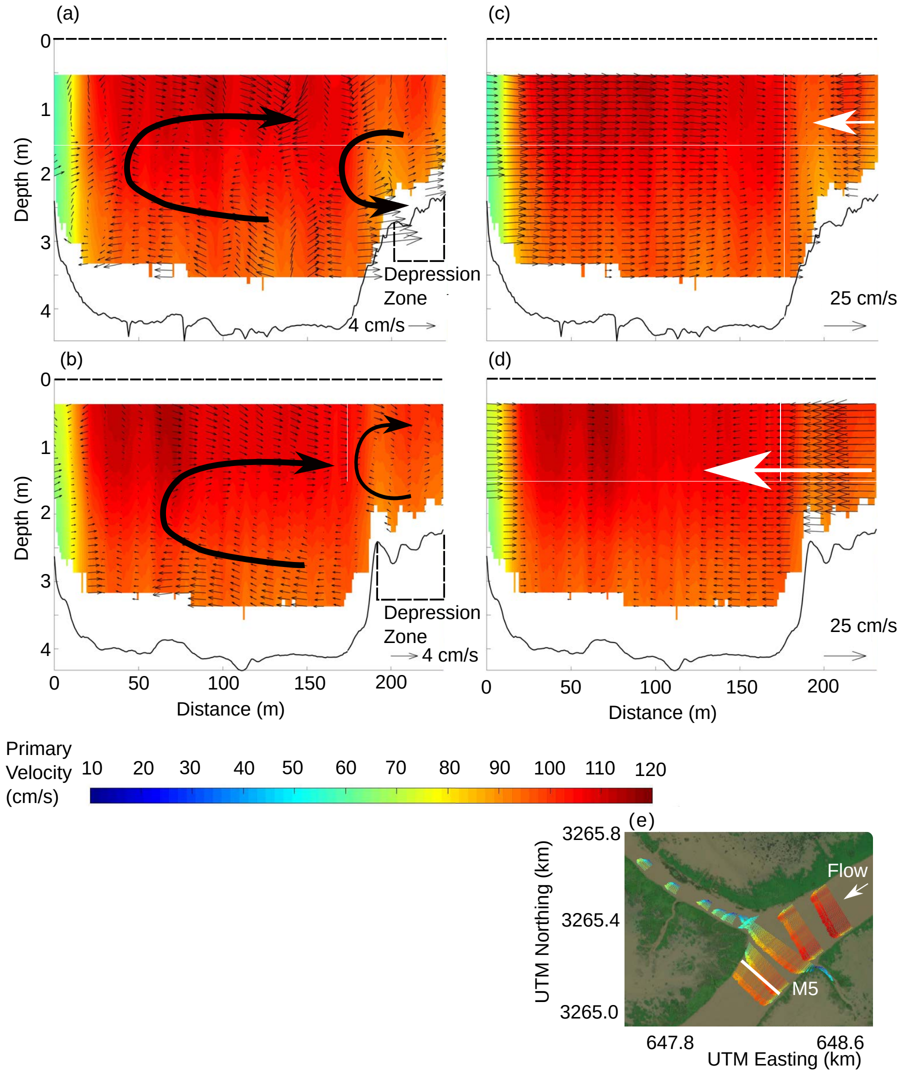

Figure 6. Flow structure and transverse velocity at transect M5, downstream of the lateral channel (looking downstream). The secondary velocities in the Rozovskii reference frame are shown by arrows and the Rozovskii primary velocities as contours in (a) and (b) from campaigns 1 (falling tide) and 2 (rising tide), respectively. The transverse velocities with primary velocities as contour from campaigns 1 and 2 are presented in (c) and (d), respectively. The inset shows the location of the transect.

A clockwise secondary circulation can also be observed in the depression zone of M4 (Fig. 5b and S2a). At transect M5, a counter-clockwise cell was observed in the depression zone during falling tide (Fig. 6a), whereas a weak clockwise cell was observed there during rising tide (Fig. 6b). A small transverse current flowing towards the main channel from the island was observed both at M4 (Fig. S2b) and M5 (Fig. 6c) during campaign 1 compared to the larger transverse current from the same direction during campaign 2 (Fig. S2d and 6d).

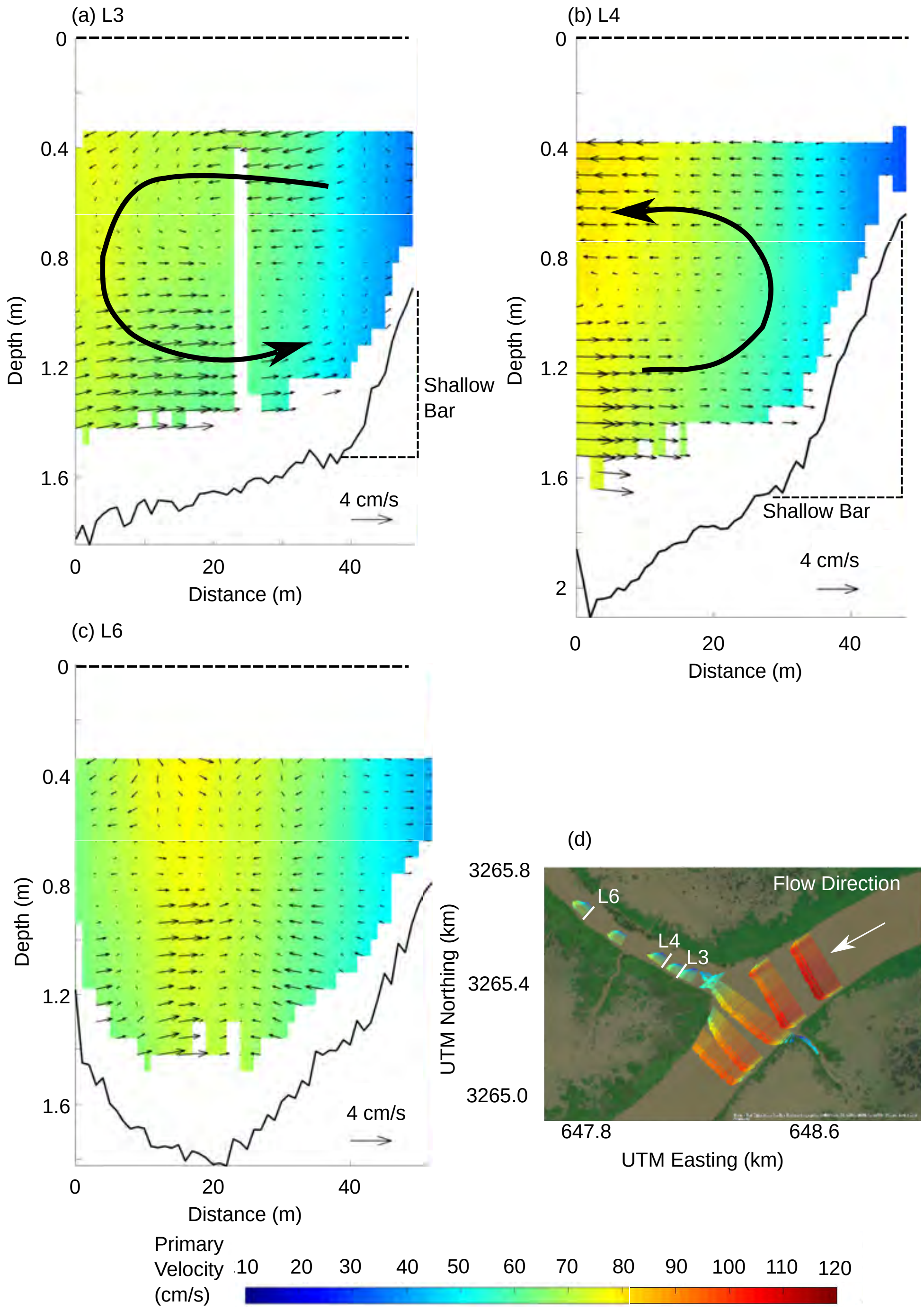

Figure 7. Flow structure at transects (a) L3, (b) L4, and (c) L6 (looking downstream). The contour shows the primary velocity and secondary velocities are shown by arrows in the Rozovskii reference frame. The velocity data was collected during campaign 2. The inset shows the location of the transects.

A coherent counter-clockwise rotating circulation cell was observed inside the lateral channel at transects L3 and L4 during both campaigns (Fig. 7a and b) accompanying a clear separation between slower flow along the right bank and faster flow along the left bank. This counter-clockwise rotating cell had a helical velocity approaching 3 cm/s that is approximately 5% of the primary velocity in the lateral channel. Farther inside the lateral channel, the coherent flow structure started to break down (Fig. 7c) as the depth gradually decreased and the high-velocity core, along with the channel thalweg, moved to the center of the lateral channel. In the rising tide survey, the circulation cell was observed to break down inside the channel at a distance 2.6-4.5 lateral channel widths (Table 1).

3.2 Unchannelized lateral outflow

Discharge and flow characteristics

Discharge at the upstream end of Gadwall Pass during campaign 3 was 388 m^3/s, which gradually decreased downstream. At transects N9 and N10, the average discharge was 229 m^3/s and 168 m^3/s, respectively. This represents a discharge loss of 37% and 54% relative to the upstream end, respectively. During campaign 4, the upstream discharge was higher (522 m^3/s) and the trend was similar until transect N10. At N10 (500 m downstream of N9) the discharge (361 m^3/s) was anomalously higher than that of N9 (278 m^3/s). A possible explanation for the increase is a lateral flux of water coming to the distributary channel near the transect from the inundated island regions due to tidal factors. The lateral outflow volume between N5-N9 was 30% of that of N5 during both campaigns. A discharge summary for UO surveys is provided in the supporting information (Fig. S3).

The average velocity at Gadwall Pass during campaign 3 was significantly lower as a consequence of smaller discharge compared to campaigns 1 and 2. During the rising tide, there was an increase in velocity near transect N7 relative to N5 (Fig. 8a). This increase might be attributed to the interaction with subaqueous channels near the transect location. The velocity core visible at the right bank of N7 gradually disappeared by transect N10, which showed 54% flow loss due to significant lateral outflow. During campaign 4 (Fig. 8b), the high-velocity core strengthened at N10 and moved towards the left bank. During campaigns 3 and 4, the Froude numbers at transect N9 were 0.031 and 0.042, respectively, and at N5 were 0.038 and 0.046, respectively. M_r' for outflow from transect N5 to N9 varied between 0.177 km^{-1} and 0.211 km^{-1} (Table 1).

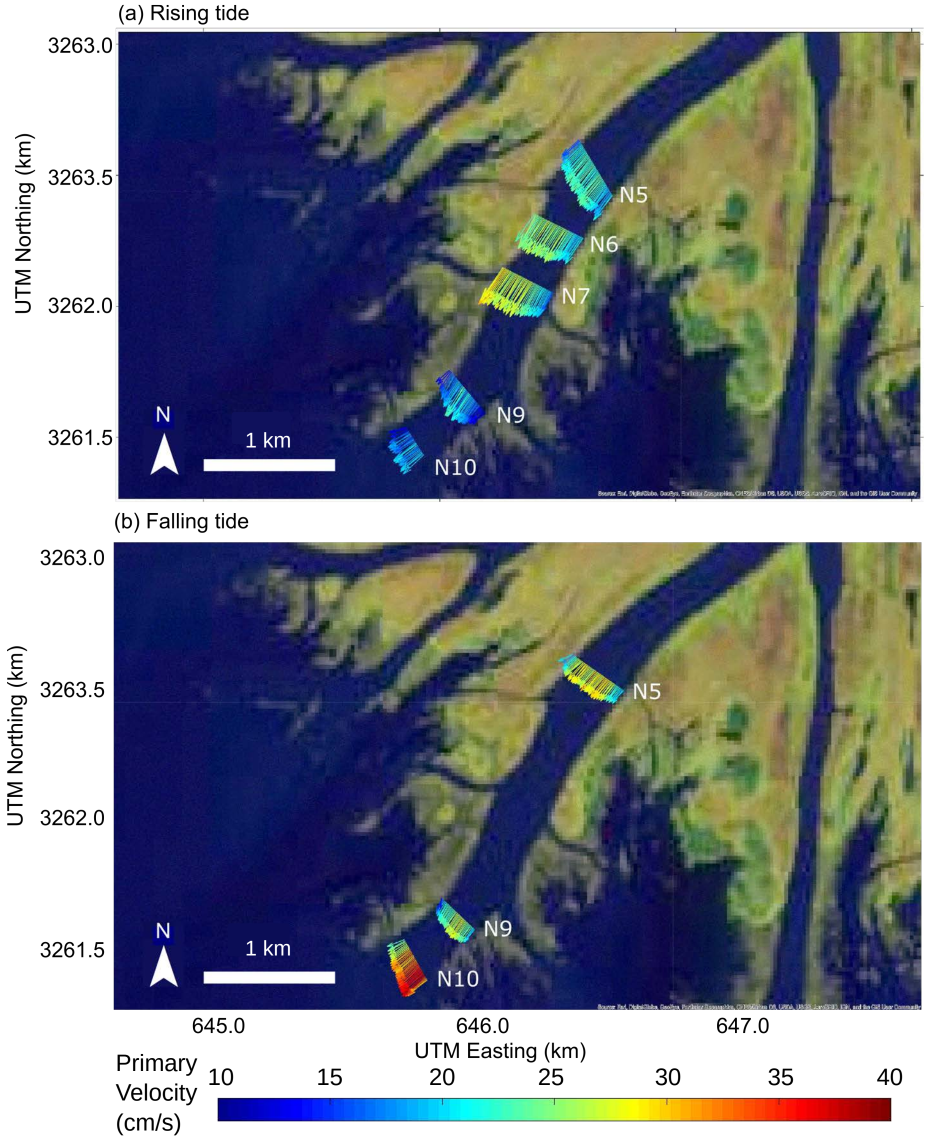

Figure 8. Depth-averaged velocity vectors along the Gadwall Pass for (a) campaign 3, rising tide, 13 September, 2019, and (b) campaign 4, falling tide, 14 September, 2019.

Flow structure

During the UO surveys in campaigns 3 and 4, no significant coherent secondary structures were observed at any of the transects downstream of N7 (Fig. 9a and b and Fig. S4). During rising tide, a loosely coherent counter-clockwise rotating structure may have existed in the middle of transect N9 (Fig. 9a), although it was not observed during falling tide (Fig. 9b). Maximum secondary velocity recorded at N9 was 2.9 cm/s. The transverse velocity near the bank was approximately 1-5 cm/s at N9 and varied in between 20-30% of mean streamwise velocity during campaign 3 and 5-20% during campaign 4. The reason behind the incoherence of flow structures might include relatively low streamwise discharge and velocity, limited curvature, differences in bed morphology, or limited exchange of momentum through the large outflow length. The transverse flow was observed to be directed from the right bank to the left bank during both campaigns 3 and 4 (Fig. S5). This suggests that tides may have an effect on the secondary structures in the unchannelized zone that may also be driven by modulation of the water-level gradient. Minimal turbulent exchange in this unconfined part of the delta has also been previously reported (Shaw et al., 2016).

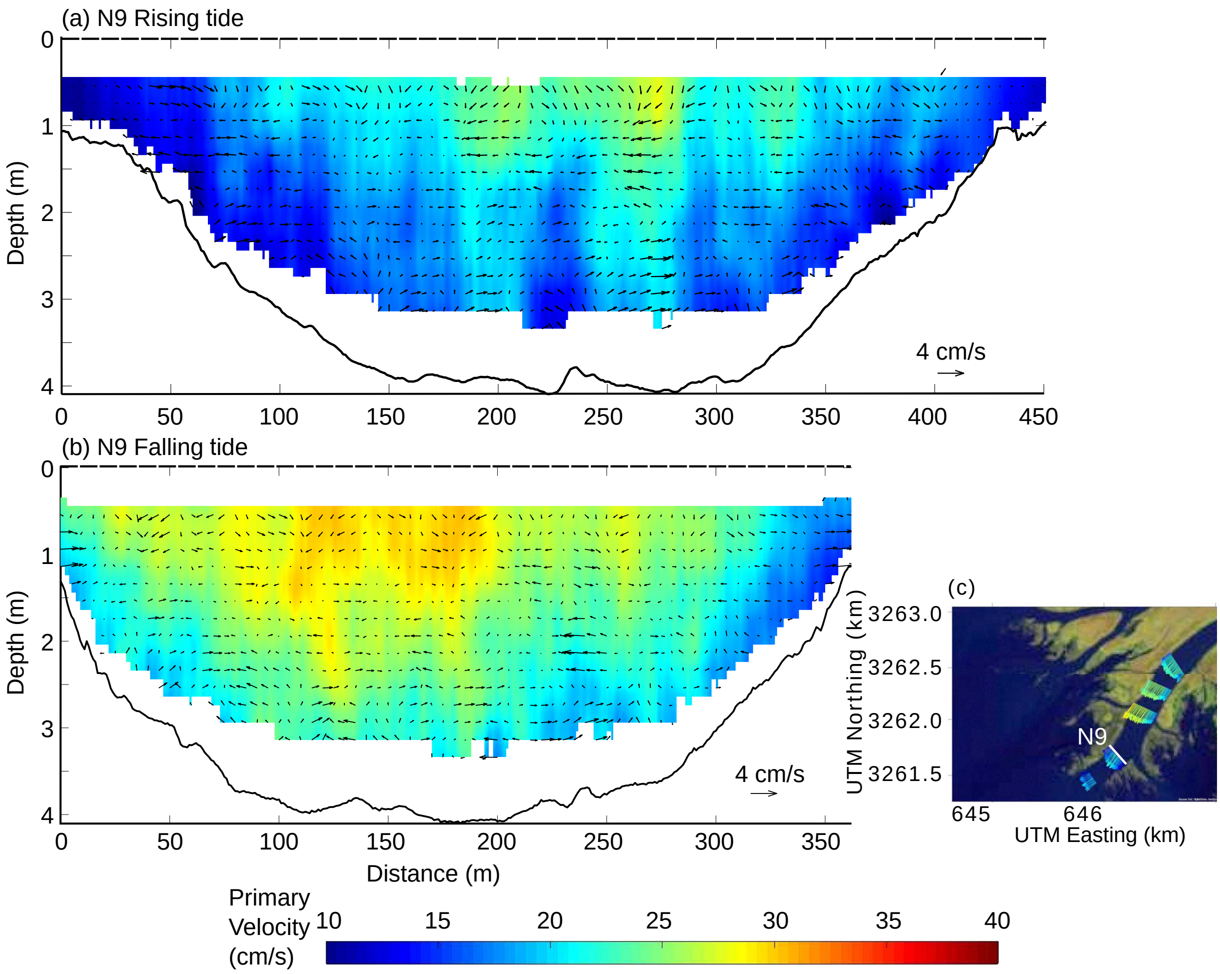

Figure 9. Flow structure at transect N9, downstream part of Gadwall Pass (looking downstream). The contour shows the primary velocity and the secondary velocities in the Rozovskii reference frame are shown by arrows for (a) campaign 3 (rising tide, 13 September 2019) and (b) campaign 4 (falling tide, 14 September, 2019). The inset shows location of the transect.

4 Discussion

Channelized lateral outflow

Time-averaged three-dimensional velocity data from the channelized outflow site (Fig. 5, 6, and 7) indicate the existence of several distinct secondary circulation cells related to lateral outflow. Inside the lateral channel which is located on the right bank of the main channel, a coherent counter-clockwise rotating cell was observed (Fig. 7a and b) along with a clockwise rotating cell at the depression zone of transect M4 (Fig. 5b). A counter-clockwise rotating cell was observed in the upstream separation zone on the right bank (Fig. 5a and c) extending upstream as far as 120m (half channel width) from the lateral channel mouth. Although the system studied here is discordant, the circulation pattern of these two cells matches previous numerical and physical modeling efforts for non-discordant 90° diversions (Neary et al., 1999; Herrero et al., 2015; Dutta et al., 2017). Cells on the depression zone away from the lateral channel (Fig. 6) were appreciably altered by transverse current (Fig. 9), and the depth-averaged velocity demonstrated some variations for different tidal regimes (Fig. 4). The circulation cells observed for channelized outflow are conceptualized in Fig. 10.

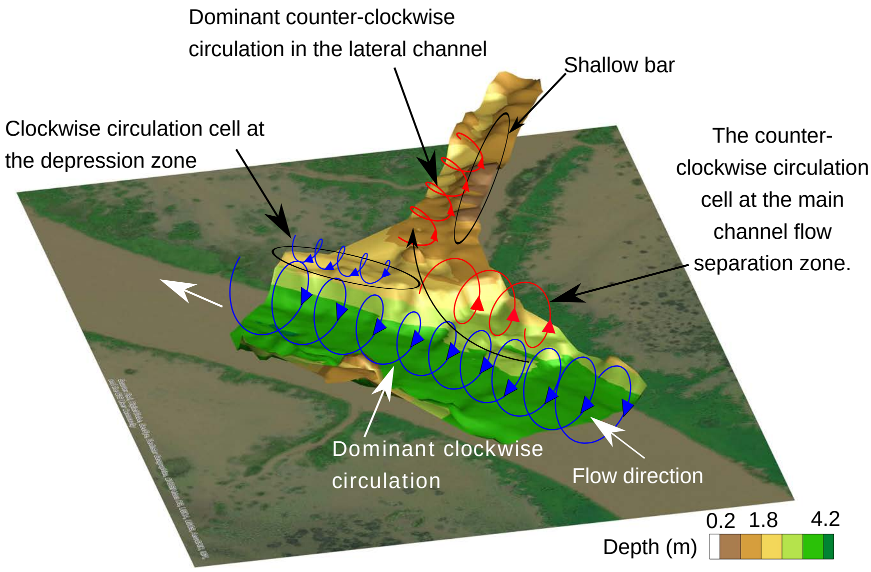

Figure 10. Conceptual figure of channelized lateral outflow

The channel-wide clockwise circulation observed in the main channel in CO survey (Fig. 5 and 6) likely represents the centre-region cell commonly observed in curved channels (Blanckaert & Vriend, 2004). This is also known to influence the transverse bed slope in river bends because the near-bed direction of the secondary flow points toward the inner bend (Rozovskii, 1957). However, in neither Mallard Pass nor Gadwall Pass do the transects along the main channel show a clear transverse bed slope. This absence of a transverse slope might be attributed to the dynamic bed development of the prograding delta and to the mild channel curvature leading to a weak center-region cell. In contrast, the transects along the lateral channel show clear transverse bed slope which are likely caused by the secondary flow (Fig. 7). Transect M3 also shows a transverse slope for the water entering the lateral channel (Fig. 5c). This slope opposes the near bed flow of the counter-clockwise cell. The effect of bed discordance and secondary flow on this transverse slope is not clear.

The observed circulation cells inside the lateral channel and downstream in the depression zone are likely the result of the imbalance between transverse pressure gradient, centrifugal forces, and shear along the vertical (Neary et al., 1999). These counter rotating cells are similar to the observation made for downstream branches in symmetric bifurcations (Miori et al., 2012; Thomas et al., 2011) and also for 90° diversions (Herrero et al., 2015).

The other coherent cell observed in the main channel is the counter-clockwise circulation near the right bank for channelized outflow. Two hypotheses can be proposed to explain its existence: 1) the circulation cells in the downstream branches (inside the lateral channel and on the depression zone) form upstream of the split point; or 2) the upstream cell represents the turbulence anisotropy and centrifugal force driven outer bank cell (Blanckaert & Vriend, 2004). It needs to be considered here that the observed structure is derived by time-averaging, and the diameter of this cell is nearly equal to the water depth. Counter-rotating circulation cells have been observed upstream of a bifurcation in models (Miori et al., 2012) which suggests two cells should also exist upstream of the lateral channel but only one was observed. In practice, it would be difficult to differentiate the clockwise rotating cell as the centre region cell also rotates in the same direction. Therefore, only the counter clockwise rotating cell could be identified. However, we do not conclude the source of the cell as outer bank cells can be persistent and may appear in weak curvature as well (Blanckaert & Vriend, 2004). Irrespective of the source, it is possible that this cell and the one inside the lateral channel act as a single continuous cell (red cells in Fig. 10).

The transverse current from islands was also observed to influence the flow structure. At transect M5, incoming water from the island on the right bank of Mallard pass was observed to alter the flow structure on the depression zone. There, a small crevasse on the right bank induced a counter-clockwise rotating cell in the channel-depression zone junction (Fig. 6a) during campaign 1. During campaign 2, instead of that cell, a faint clockwise rotating secondary structure on the depression zone was observed (Fig. 6b). The transverse velocity vectors (Fig. 6d) indicate a large transverse current moving from the floodplain to the channel compared to the smaller transverse flow during campaign 1 (Fig. 6c). A similar observation was made at transect M4 (Fig. S3) showing a larger transverse current moving into the main channel during campaign 2 (Fig. S3d), but the clockwise circulation direction on the depression zone remained unchanged during both campaigns (Fig. S3a and c). It is unclear why the transverse current had less effect at M4 but the non existence of the crevasse induced counter-clockwise circulation at M5 (Fig. 6b) suggests that transverse currents can potentially modify existing secondary currents under suitable conditions.

To provide an estimate of the size of particles that can be influenced by the observed secondary flow structure, the settling velocity of the median grain size at WLD and the secondary velocities were compared. It should be noted here that most of the transport indeed is driven by the shear stress of the primary flow, while the observed coherent structures act to deviate the transport direction from the primary flow direction, potentially bringing sediment to the interdistributary islands. For the WLD's mean median grain size at apex of $106\mu m$ (Shaw et al., 2013) the settling velocity is approximately 0.8 cm/s (for formulation see e-book by Parker (2004)). The counter-clockwise rotating coherent circulation velocity for the channelized outflow was fluctuating in between 2-4 cm/s (Fig. 5a). Therefore, it is an order of magnitude greater than the settling velocity and thus may influence the transport direction of the median sized particles in suspension into the lateral channel. Based on this simple calculation and maximum velocity observed in the structure, this cell may deviate grains of size up to 200 μm. However, direct observations of the influence of secondary flow structure on modulating sediment transport in the field remains lacking and is an avenue warranting further study.

This study featured field observations of flow structure in a discordant lateral outflow, which has yet to be observed in detail. The flow structures observed in this study are similar to those observed in previous non-discordant diversion studies (Neary et al., 1999; Herrero et al., 2015; Dutta et al., 2017). A shallow elongated bar was observed inside the lateral channel (Fig. 3) which is similar to previous observations in non-discordant systems (Bulle, 1926; Herrero et al., 2015; Szewczyk et al., 2020). The reproduction of flow structure and the presence of the shallow bar in the CO study, suggest that the Bulle effect (Bulle, 1926), i.e., preferential deviation of bedload sediment into the lateral branch because of the secondary circulation at the mouth, may also take place in discordant lateral channels in deltas gradually filling up the channel. Kästner and Hoitink (2019) suggested that narrow, discordant branches should induce stronger circulation in the diverted flow than a non-discordant lateral outflow with equal-width main channels, but direct observations to test this statement are currently unavailable in this study.

Unchannelized lateral outflow

For unchannelized outflow, no coherent circulation was observed, at least in the most downstream parts of the channel. Transects upstream of N7 (Fig. S4) do show weak but large clockwise circulation reaching 3 cm/s likely representing the helical flow induced by the slight curvature of Gadwall pass. At these transects, the lateral outflow was fairly small (Table S7). At transect N9 where the discharge loss was around 30% of that of N5, secondary structures appeared to be weak and incoherent (Fig. 9). Flow structure at this transect appeared to vary with tidal stages.

Unchannelized lateral outflow is functionally similar to channelized outflow in that water volume and momentum are lost by the main channel, albeit the length over which lateral outflow occurs is several times larger than the main channel width. Secondary flow velocity scales directly with primary flow velocity and inversely with radius of curvature (De Vriend, 1977; Rozovskii, 1957) which is roughly proportional to the length of outflow. For this case, the primary velocity was roughly three times smaller, whereas the radius of curvature was several times larger than in the channelized case. Thus, the lack of circulation cells during campaigns 3 and 4 at N9 and N10 is expected due to low velocities in the main channel resulting from relatively low upstream discharge and long zone of lateral outflow. Similar phenomena were also observed by Shaw et al. (2016) who suggested that the lateral turbulent mixing from the unstable flow was minimal in the subaqueous region of WLD. Though no coherent secondary structures were observed for the UO portion of the delta for the conditions studied, the authors hypothesize that there may be considerable lateral momentum flux under high flow conditions that may induce secondary flows in the distributary channels. Such secondary structures have been observed in the main channel-floodplain junction of compound channels in experimental studies (Branß et al., 2016; Tominaga & Nezu, 1991; Proust & Nikora, 2019). More comprehensive measurements covering a range of discharges in the field coupled with three-dimensional hydrodynamic modeling would be required to address this hypothesis.

Outflow momentum flux

The momentum flux ratio, M_r, quantifies the momentum departing the main channel flow as a result of lateral outflow (Herrero et al., 2015). Previous observations found a threshold M_r of 0.04 for the formation of vertical structures in the depression zone of a 90° diversion (Herrero et al., 2015). For the current study, the bathymetry of transects M4 and M5 (Fig. 3) also suggests a depression zone on the right bank downstream of the lateral channel. During campaigns 1 and 2, M_r was calculated as 0.04 and 0.03 respectively for the CO system (Table 1), which compares favorably to the previous observations of Herrero et al. (2015).

The value of M_r in a delta channel may vary with discharge, tides, and storms. However, the system studied here is different from most of the experimental and modeling studies with a discordant lateral branch that is at least three times smaller in width than the main channel. Previous studies mostly focused on systems with non-discordant bed with equal branch width. The secondary cells observed in our study (Fig. 6) suggest inlet geometry, particularly the length of outflow zone, plays a vital role in a deltaic environment compare to what the experiments suggest. Recent field studies have demonstrated that inlets to the branches with larger cross sectional area decrease the strength of the secondary circulation in the diverted flow (Kästner & Hoitink, 2019). This suggests that circulations in the distributed lateral outflow would be much weaker as the outflow occurs over a larger length than that of a channelized system. In addition, the ratios of outflow velocity and mean streamwise velocity near the banks for UO and CO in some cases were observed to be of similar magnitude (M3 during campaign 1, 30%, and N9 during campaign 3, 20-30%). Despite the ratios in two outflow systems being similar, coherent circulations were apparent only in CO but not in UO. The velocity ratio in the equation of M_r (eq. 1) thus may not provide the threshold for coherent secondary cell formation as it does not contain the outflow length information. It is therefore essential to modify the previously defined momentum flux ratio to incorporate the length of outflow zone to address the secondary flow threshold for both channelized and unchannelized outflow in a delta.

The outflow momentum flux ratio M_r' introduced herein is a modified version of M_r that includes the length scale of lateral outflow in its calculation (Eq. 3). This is useful because the length scale of lateral outflow and the momentum flux are both hypothesized to exert control on the formation of secondary flow structures. The outflow momentum flux ratio is a useful metric as it can be used as a representative parameter of secondary flow structures in 1D morphodynamic models of bifurcations which often have to ignore the spiral flow that are inherently three-dimensional (Van der Mark & Mosselman, 2012). Having such in these models would provide a tool to incorporate the effects of secondary flow structures on the morphology in an efficient manner.

In the current study, for unchannelized outflow the value of M_r' considering transects N5 to N9 was found to be between 0.177 and 0.211 km^{-1} with no coherent circulation observed at the main channel-floodplain junction. Whereas, for channelized outflow, M_r' in the two campaigns were significantly higher varying between 0.375 and 0.492 km^{-1} and coherent secondary currents were observed in both cases. Comparing the calculated M_r' for both CO and UO surveys, we hypothesize that the threshold for the formation of coherent secondary circulation may lie in between M_r' values of 0.211 km^{-1} and 0.375 km^{-1}. The prediction is rough and more measurements during intermediate discharge conditions along with using a three-dimensional hydrodynamic model will provide a more precise range for the threshold.

The M_r' formulation used in this study was constrained by the conditions observed at WLD. According to channel bifurcation literature (e.g., Kästner & Hoitink, 2019; Kästner & Hoitink, 2020; Szupiany et al., 2012), channel width-depth ratio influences the strength of secondary flow. In this study, due to the diffuse nature of the UO, depth was not included in the formulation of M_r'. Depth changes significantly over the length of the UO region, thus complicating the selection of a representative depth. It is likely that channel depth and depth of the outflow over the channel banks in UO may have some impact on the presence and strength of the secondary flow, but studies capturing variations in flow depth are required to address this problem. In addition, the allocation of UO between the two flanking floodplains may vary along the length of a single channel and is likely significantly variable across channels and sites. Thus, the impacts of flow over both banks, over just one bank, and the spatial variability of this interaction all likely play controlling roles in the patterns of secondary flow. Therefore, avenues for further research may also include defining the M_r' threshold for UO evaluating the relative significance of flow depth and outflow length on the formation of secondary structures.

Morphology

It was previously shown in field (Kästner & Hoitink, 2019) and experimental (Herrero et al., 2015; Onen & Agaccioglu, 2013) studies that lateral outflow from the outer bank of a channel bend results in a scour hole in the outer bank of the main channel downstream of the outflow. In our interpolated bathymetry, we did not observe any such scour, which could be due to the coarse bathymetric grid. Near bed sediment extraction at a greater ratio than diverted water (Bulle, 1926; Kästner & Hoitink, 2019) may cause a scour to form, which also results in deposition along the inner bank as flow is lost due to outflow. Nevertheless, in our case, we propose two hypotheses that may explain the lack of evidence of a scour: 1) during high discharge events, the delta is mostly depositional and experiences channel bed aggradation thus potentially filling in a previous scour (Shaw & Mohrig, 2014); and 2) because of the bed level discordance, the steep transverse bed slope causes bedload to stay preferentially in the main channel (Bolla Pittaluga et al., 2003). Higher resolution topography and modeling exercises resolving bed level change may address these hypotheses.

5 Conclusions

This study presents field data quantifying the effect of lateral outflow on the three-dimensional flow structure in the distributary channels of a river dominated delta (Wax Lake Delta in coastal Louisiana, USA). Several recent studies have concluded that such lateral outflow is critical for deltaic maintenance, growth, and morphodynamic evolution. This study provides novel observations and analyses of hydrodynamics influencing transport processes in a prograding river delta that is a prototype for restoration via river diversions. Thus it has significant implications for coastal restoration efforts aimed at mitigating coastal wetland loss.

Hydrographic surveys were performed using an acoustic Doppler current profiler (ADCP) to map the flow structure and bathymetry of two sites typifying channelized and unchannelized outflow zones in a prograding river delta. In the channelized outflow site, four coherent secondary structures were observed in the time-averaged flow field at both rising and falling tide. However, no significant coherent secondary circulations were observed for the site experiencing lateral overbank outflow. Transverse currents from the floodplain were observed to impact flow patterns. The coherent circulation cells are directly linked to the patterns in bed morphology.

A threshold outflow momentum flux ratio is proposed in this study to quantify the impact of the lateral outflow type (channelized or unchannelized) on the formation and coherence of secondary flow structures in deltaic distributary channels. The outflow momentum flux ratio is quantified as the ratio of momentum flux in the main distributary flow to the lateral outflow normalized by the length of the lateral outflow zone. Calculated values lie between 0.177 km^{-1} and 0.492 km^{-1} for the observed conditions. Secondary flow structures were observed in the distributary channels for values above 0.375 km^{-1}.

The results from this study suggest that the maximum grain size of suspended sediments carried inside the lateral channel may depend on the strength of the secondary circulation cell in the upstream separation zone which is dependent upon the outflow momentum flux ratio. Particle settling velocity calculations indicate that the observed outflow induced coherent circulation cells induced by channelized outflow are capable of influencing transport of suspended particles of up to 200 μm into the lateral channel. The flow structure in the unchannelized zone was found to be incoherent as the momentum transfer typically occurs over a large distance, unlike the smaller outflow length in the case of channelized outflow. As water moves downstream from the delta apex, the available flow momentum drops because of lateral outflow and bed friction, likely leading to simultaneously different transport conditions at different parts of the delta. In this context, the outflow momentum flux ratio provides estimates of the sediment grain size being transported in the different zones of the distributary system for a given water discharge condition.

6 Data Availability Statement

The discharge and waterlevel data can be found at https://waterdata.usgs.gov/ and https://tidesandcurrents.noaa.gov/, respectively. The ADCP data used in this article are available via figshare repository https://doi.org/10.6084/m9.figshare.15094149.v1 in ASCII text and .mat file format for using in Velocity Mapping Toolbox (VMT) with Attribution 4.0 International (CC BY 4.0) license (Chowdhury et al., 2021).

References

Bevington, A. E., & Twilley, R. R. (2018). Island edge morphodynamics along a chronosequence in a prograding deltaic floodplain wetland. *Journal of Coastal Research*, *344*, 806–817. doi: 10.2112/jcoastres-d-17-00074.1

Blanckaert, K., & Vriend, H. J. D. (2004). Secondary flow in sharp open-channel bends. *Journal of Fluid Mechanics*, *498*, 353–380. doi: 10.1017/s0022112003006979

Bolla Pittaluga, M., Repetto, R., & Tubino, M. (2003). Channel bifurcation in braided rivers: Equilibrium configurations and stability. *Water Resour. Res.*, *39*. doi: 10.1029/2001WR001112

Branß, T., Dittrich, A., & Núñez-González, F. (2016). Reproducing natural levee formation in an experimental flume. In *River flow 2016.* CRC Press. doi: 10.1201/9781315644479-178

Bulle, H. (1926). *Untersuchungen über die geschiebeableitung bei der spaltung von wasserläufen: Modellversuche aus dem flussbaulaboratorium der technischen hochschule zu karlsruhe.* VDI-Verlag.

Buschman, F. A., van der Vegt, M., Hoitink, A. J. F., & Hoekstra, P. (2013). Water and suspended sediment division at a stratified tidal junction. *Journal of Geophysical Research: Oceans*, *118*(3), 1459-1472. doi: https://doi.org/10.1002/jgrc.20124

Chowdhury, M. K. (2020). *akifayath/teledyne-adcp-tilt-correction: Adcp tilt correction.* Zenodo. doi: 10.5281/ZENODO.3759971

Chowdhury, M. K., Hiatt, M., & Konsoer, K. M. (2021). *Effect of lateral outflow on flow structure in a river delta.* figshare. doi: https://doi.org/10.6084/m9.figshare.15094149.v1

Christensen, A., Twilley, R. R., Willson, C. S., & Castañeda-Moya, E. (2020). Simulating hydrological connectivity and water age within a coastal deltaic floodplain of the Mississippi River Delta. *Estuarine, Coastal and Shelf Science*, *245*, 106995. doi: https://doi.org/10.1016/j.ecss.2020.106995

Coffey, T. S., & Shaw, J. B. (2017). Congruent bifurcation angles in river delta and tributary channel networks. *Geophysical Research Letters*, n/a–n/a. (2017GL074873) doi: 10.1002/2017GL074873

CPRA. (2017). *Louisiana's Comprehensive Master Plan for a Sustainable Coast* (Technical Report). Baton Rouge, LA: The State of Louisiana.

De Vriend, H. J. (1977). A mathematical model of steady flow in curved shallow channels. *Journal of Hydraulic Research*, *15*(1), 37–54. doi: 10.1080/00221687709499748

Dutta, S., Wang, D., Tassi, P., & Garcia, M. H. (2017). Three-dimensional numerical modeling of the Bulle effect: the nonlinear distribution of near-bed sediment at fluvial diversions. *Earth Surface Processes and Landforms*, *42*(14), 2322–2337. doi: 10.1002/esp.4186

Edmonds, D. A., Paola, C., Hoyal, D. C. J. D., & Sheets, B. A. (2011). Quantitative metrics that describe river deltas and their channel networks. *Journal of Geophysical Research*, *116*(F4). doi: 10.1029/2010jf001955

Engel, F. L., & Rhoads, B. L. (2017). Velocity profiles and the structure of turbulence at the outer bank of a compound meander bend. *Geomorphology*, *295*, 191–201. doi: 10.1016/j.geomorph.2017.06.018

Esposito, C. R., Georgiou, I. Y., & Straub, K. M. (2020). Flow loss in deltaic distributaries: Impacts on channel hydraulics, morphology and stability. *Water Resources Research*. doi: 10.1029/2019wr026463

Finotello, A., Ghinassi, M., Carniello, L., Belluco, E., Pivato, M., Tommasini, L., & D'Alpaos, A. (2020). Three-dimensional flow structures and morphodynamic evolution of microtidal meandering channels. *Water Resources Research*, *56*(7), e2020WR027822. doi: https://doi.org/10.1029/2020WR027822

Frothingham, K. M., & Rhoads, B. L. (2003). Three-dimensional flow structure and channel change in an asymmetrical compound meander loop, Embarras River, Illinois. *Earth Surface Processes and Landforms: The Journal of the British Geomorphological Research Group*, *28*(6), 625–644.

Hardy, R. J., Lane, S. N., & Yu, D. (2011). Flow structures at an idealized bifurcation: a numerical experiment. *Earth Surface Processes and Landforms*, *36*(15), 2083–2096. doi: 10.1002/esp.2235

Herrero, A., Bateman, A., & Medina, V. (2015). Water flow and sediment transport in a 90°channel diversion: an experimental study. *Journal of Hydraulic Research*, *53*(2), 253–263. doi: 10.1080/00221686.2014.989457

Hiatt, M., Castañeda-Moya, E., Twilley, R., Hodges, B. R., & Passalacqua, P. (2018). Channel-island connectivity affects water exposure time distributions in a coastal river delta. *Water Resources Research*, *54*(3), 2212-2232. doi: https://doi.org/10.1002/2017WR021289

Hiatt, M., & Passalacqua, P. (2015). Hydrological connectivity in river deltas: The first-order importance of channel-island exchange. *Water Resour. Res.*, *51*, 2264-2282. doi: 10.1002/2014WR016149

Hiatt, M., & Passalacqua, P. (2017). What controls the transition from confined to unconfined flow? analysis of hydraulics in a coastal river delta. *Journal of Hydraulic Engineering*, *143*(6), 03117003. doi: 10.1061/(asce)hy.1943-7900.0001309

Kästner, K., & Hoitink, A. (2020). Idealized model for the deflection of sediment into lateral branches of lowland rivers. *Water Resources Research*, *56*(6), e2019WR026602.

Kim, W., Mohrig, D., Twilley, R., Paola, C., & Parker, G. (2009). Is it feasible to build new land in the Mississippi River Delta? *Eos, Transactions American Geophysical Union*, *90*(42), 373–374. doi: 10.1029/2009eo420001

Konsoer, K. M., Rhoads, B. L., Best, J. L., Langendoen, E. J., Abad, J. D., Parsons, D. R., & Garcia, M. H. (2016). Three-dimensional flow structure and bed morphology in large elongate meander loops with different outer bank roughness characteristics. *Water Resources Research*, *52*(12), 9621–9641. doi: 10.1002/2016wr019040

Kästner, K., & Hoitink, A. J. F. (2019). Flow and suspended sediment division at two highly asymmetric bifurcations in a river delta: Implications for channel stability. *Journal of Geophysical Research: Earth Surface*, *124*(10), 2358-2380.

Lane, S. N., Bradbrook, K., Richards, K., Biron, P., & Roy, A. (2000). Secondary circulation cells in river channel confluences: measurement artefacts or coherent flow structures? *Hydrological Processes*, *14*(11-12), 2047–2071.

Marra, W. A., Parsons, D. R., Kleinhans, M. G., Keevil, G. M., & Thomas, R. E. (2014). Near-bed and surface flow division patterns in experimental river bifurcations. *Water Resources Research*, *50*(2), 1506–1530. doi: 10.1002/2013wr014215

Michelazzo, G., Minatti, L., Paris, E., & Solari, L. (2016). Side weir flow on a movable bed. *Journal of Hydraulic Engineering*, *142*(6), 04016007. doi: 10.1061/(ASCE)HY.1943-7900.0001128

Michelazzo, G., Oumeraci, H., & Paris, E. (2015). Laboratory study on 3D flow structures induced by zero-height side weir and implications for 1D Modeling. *Journal of Hydraulic Engineering*, *141*(10), 04015023. doi: 10.1061/(ASCE)HY.1943-7900.0001027

Miori, S., Hardy, R. J., & Lane, S. N. (2012). Topographic forcing of flow partition and flow structures at river bifurcations. *Earth Surface Processes and Landforms*, *37*(6), 666–679. doi: 10.1002/esp.3204

Miyawaki, S., Constantinescu, G., Rhoads, B., & Sukhodolov, A. (2010). Changes in three-dimensional flow structure at a river confluence with changes in momentum ratio. In *River flow* (Vol. 2010, pp. 225–232).

Mueller, D., Wagner, C., Rehmel, M., Oberg, K., & Rainville, F. (2013). Measuring discharge with acoustic Doppler current profilers from a moving boat (ver. 2.0, December 2013): US Geological Survey Techniques and Methods, book 3, chap. A22. , 95. (available at https://pubs.usgs.gov/tm/3a22/)

Neary, V. S., & Odgaard, A. J. (1993). Three-dimensional flow structure at open-channel diversions. *Journal of Hydraulic Engineering*, *119*(11), 1223–1230.

Neary, V. S., Sotiropoulos, F., & Odgaard, A. J. (1999). Three-dimensional numerical model of lateral-intake inflows. *Journal of Hydraulic Engineering*, *125*(2), 126–140. doi: 10.1061/(asce)0733-9429(1999)125:2(126)

Nezu, I., & Onitsuka, K. (2001). Turbulent structures in partly vegetated open-channel flows with LDA and PI v measurements. *Journal of Hydraulic Research*, *39*(6), 629–642. doi: 10.1080/00221686.2001.9628292

O'Connor, M. T., & Moffett, K. B. (2015). Groundwater dynamics and surface water–groundwater interactions in a prograding delta island, Louisiana, USA. *Journal of Hydrology*, *524*, 15 - 29. doi: http://dx.doi.org/10.1016/j.jhydrol.2015.02.017

Olliver, E. A., Edmonds, D. A., & Shaw, J. B. (2020). Influence of floods, tides, and vegetation on sediment retention in wax lake delta, louisiana, USA. *Journal of Geophysical Research: Earth Surface*, *125*(1). doi: 10.1029/2019jf005316

Onen, F., & Agaccioglu, H. (2013). Live bed scour at a side-weir intersection located on an alluvial channel. *Irrigation and Drainage*, n/a–n/a. doi: 10.1002/ird.1749

Pal, S., Lee, T. R., & Clark, N. E. (2020). The 2019 Mississippi and Missouri River flooding and its impact on atmospheric boundary layer dynamics. *Geophysical Research Letters*, *47*(6). doi: 10.1029/2019gl086933

Paris, E., Solari, L., & Bechi, G. (2012). Applicability of the De Marchi hypothesis for side weir flow in the case of movable beds. *Journal of Hydraulic Engineering*, *138*(7), 653-656. doi: 10.1061/(ASCE)HY.1943-7900.0000566

Parker, G. (2004). *1d sediment transport morphodynamics with applications to rivers and turbidity currents* (Vol. 13).

Parsons, D. R., Jackson, P. R., Czuba, J. A., Engel, F. L., Rhoads, B. L., Oberg, K. A., ... Riley, J. D. (2013). Velocity mapping toolbox (VMT): a processing and visualization suite for moving-vessel ADCP measurements. *Earth Surface Processes and Landforms*, *38*(11), 1244–1260. doi: 10.1002/esp.3367

Passalacqua, P. (2017). The delta connectome: A network-based framework for studying connectivity in river deltas. *Geomorphology*, *277*, 50–62. doi: 10.1016/j.geomorph.2016.04.001

Proust, S., & Nikora, V. I. (2019). Compound open-channel flows: effects of transverse currents on the flow structure. *Journal of Fluid Mechanics*, *885*. doi: 10.1017/jfm.2019.973

Ramamurthy, A. S., Qu, J., & Vo, D. (2007). Numerical and experimental study of dividing open-channel flows. *Journal of Hydraulic Engineering*, *133*(10), 1135–1144. doi: 10.1061/(asce)0733-9429(2007)133:10(1135)

Rennie, C. D., & Church, M. (2010). Mapping spatial distributions and uncertainty of water and sediment flux in a large gravel bed river reach using an acoustic Doppler current profiler. *Journal of Geophysical Research*, *115*(F3). doi: 10.1029/2009jf001556

Rhoads, B. L., & Kenworthy, S. T. (1998). Time-averaged flow structure in the central region of a stream confluence. *Earth Surface Processes and Landforms: The Journal of the British Geomorphological Group*, *23*(2), 171–191.

Rhoads, B. L., & Sukhodolov, A. N. (2001). Field investigation of three-dimensional flow structure at stream confluences: 1. thermal mixing and time-averaged velocities. *Water Resources Research*, *37*(9), 2393–2410. doi: 10.1029/2001wr000316

Roberts, H. (1998). Delta switching: early responses to the Atchafalaya River diversion. *Journal of Coastal Research*, *14*(3).

Roberts, H., Coleman, J., Bentley, S., & Walker, N. (2003). An embryonic major delta lobe: A new generation of delta studies in the Atchafalaya-Wax Lake Delta system.

Roberts, H., Walker, N., Cunningham, R., Kemp, G., & Majersky, S. (1997). Evolution of sedimentary architecture and surface morphology: Atchafalaya and Wax Lake Deltas, Louisiana (1973-1994).

Rosier, B., Boillat, J.-L., & Schleiss, A. J. (2011). Influence of lateral water withdrawal on bed form geometry in a channel. *Journal of Hydraulic Engineering*, *137*(12), 1668–1675. doi: 10.1061/(asce)hy.1943-7900.0000472

Rozovskii, I. (1957). Flow of water in bends of open channels (in Russian), 233 pp. *Acad. of Sci. of the Ukrainian SSR, Kiev.(English translation, Isr. Program for Sci. Transl., Jerusalem, 1961.)*.

Sassi, M. G., Hoitink, A. J. F., Vermeulen, B., & Hidayat, H. (2013). Sediment discharge division at two tidally influenced river bifurcations. *Water Resources Research*, *49*(4), 2119-2134. doi: https://doi.org/10.1002/wrcr.20216

Serres, B. D., Roy, A. G., Biron, P. M., & Best, J. L. (1999). Three-dimensional structure of flow at a confluence of river channels with discordant beds. *Geomorphology*, *26*(4), 313–335. doi: 10.1016/s0169-555x(98)00064-6

Shaw, J., Estep, J. D., Whaling, A. R., Sanks, K. M., & Edmonds, D. A. (2018). Measuring subaqueous progradation of the Wax Lake Delta with a model of flow direction divergence. *Earth Surface Dynamics*, *6*(4), 1155–1168. doi: 10.5194/esurf-6-1155-2018

Shaw, J., & Mohrig, D. (2014). The importance of erosion in distributary channel network growth, Wax Lake Delta, Louisiana, USA. *Geology*, *42*, 31-34. doi: 10.1130/G34751.1

Shaw, J., Mohrig, D., & Wagner, R. W. (2016). Flow patterns and morphology of a prograding river delta. *Journal of Geophysical Research: Earth Surface*, *121*(2), 372–391. doi: 10.1002/2015JF003570

Shaw, J., Mohrig, D., & Whitman, S. (2013). The morphology and evolution of channels on the Wax Lake Delta, Louisiana, USA. *J. Geophys. Res.: Earth Surf.*, *108*. doi: 10.1002/jgrf.20123

Sukhodolov, A. N. (2012). Structure of turbulent flow in a meander bend of a lowland river. *Water Resources Research*, *48*(1). doi: 10.1029/2011wr010765

Szewczyk, L., Grimaud, J.-L., & Cojan, I. (2020). Experimental evidence for bifurcation angles control on abandoned channel fill geometry. *Earth Surface Dynamics*, *8*(2), 275–288. doi: 10.5194/esurf-8-275-2020

Szupiany, R. N., Amsler, M. L., Best, J. L., & Parsons, D. R. (2007). Comparison of fixed- and moving-vessel flow measurements with an aDp in a large river. *Journal of Hydraulic Engineering*, *133*(12), 1299–1309. doi: 10.1061/(asce)0733-9429(2007)133:12(1299)

Szupiany, R. N., Amsler, M. L., Hernandez, J., Parsons, D. R., Best, J. L., Fornari, E., & Trento, A. (2012). Flow fields, bed shear stresses, and suspended bed sediment dynamics in bifurcations of a large river. *Water Resources Research*, *48*(11). doi: 10.1029/2011wr011677

Szupiany, R. N., Amsler, M. L., Parsons, D. R., & Best, J. L. (2009). Morphology, flow structure, and suspended bed sediment transport at two large braid-bar confluences. *Water Resources Research*, *45*(5). doi: 10.1029/2008wr007428

Teledyne, R. I. (2010). Adcp coordinate transformation: formulas and calculations. *TELEDYNE RD INSTRUMENTS, Technical manual*.

Teledyne, R. I. (2017). Riverpro & Riopro ADCP guide [Computer software manual].

Thomas, R. E., Parsons, D. R., Sandbach, S. D., Keevil, G. M., Marra, W. A., Hardy, R. J., ... Ross, J. A. (2011). An experimental study of discharge partitioning and flow structure at symmetrical bifurcations. *Earth Surface Processes and Landforms*, *36*(15), 2069–2082. doi: 10.1002/esp.2231

Tominaga, A., & Nezu, I. (1991). Turbulent structure in compound open-channel flows. *Journal of Hydraulic Engineering*, *117*(1), 21–41. doi: 10.1061/(asce)0733-9429(1991)117:1(21)

Uijttewaal, W. S. (2014). Hydrodynamics of shallow flows: application to rivers. *Journal of Hydraulic Research*, *52*(2), 157–172. doi: 10.1080/00221686.2014.905505

Van der Mark, C. F., & Mosselman, E. (2012). Effects of helical flow in one-dimensional modelling of sediment distribution at river bifurcations. *Earth Surface Processes and Landforms*, *38*(5), 502–511. doi: 10.1002/esp.3335

Venditti, J. G., Rennie, C. D., Bomhof, J., Bradley, R. W., Little, M., & Church, M. (2014). Flow in bedrock canyons. *Nature*, *513*(7519), 534–537. doi: 10.1038/nature13779

Wellner, R., Beaubouef, R., Van Wagoner, J., Roberts, H., & Sun, T. (2005). Jet-plume depositional bodies—the primary building blocks of Wax Lake Delta.

Wright, K., Hiatt, M., & Passalacqua, P. (2018). Hydrological connectivity in vegetated river deltas: The importance of patchiness below a threshold. *Geophysical Research Letters*, *45*(19), 10,416-10,427. doi: 10.1029/2018GL079183

Zinger, J. A., Rhoads, B. L., Best, J. L., & Johnson, K. K. (2013). Flow structure and channel morphodynamics of meander bend chute cutoffs: A case study of the Wabash River, USA. *Journal of Geophysical Research: Earth Surface*, *118*(4), 2468–2487. doi: 10.1002/jgrf.20155

Zolezzi, G., Bertoldi, W., Tubino, M., Smith, G., Best, J., Bristow, C., & Petts, G. (2006). Morphological analysis and prediction of river bifurcations. *Braided rivers: process, deposits, ecology and management*, *36*, 233–256.